

Original article

Flexible computational docking studies of new aminoglycosides targeting RNA 16S bacterial ribosome site

Florent Barbault^{a,*}, Bo Ren^b, Joseph Rebehmed^a, Catia Teixeira^a, Yun Luo^a,
Ornella Smila-Castro^a, François Maurel^a, BoTao Fan^{a,✕}, Liangren Zhang^{b,**}, Lihe Zhang^b^a ITODYS, Université Paris Diderot, CNRS UMR 7086, 1 rue Guy de la Brosse, 75005 Paris, France^b State Key Laboratory of Natural and Biomimetic Drugs, School of Pharmaceutical Sciences, Peking University, Beijing 100083, China

Received 21 June 2007; received in revised form 8 October 2007; accepted 11 October 2007

Available online 22 October 2007

Abstract

Ribonucleic acids (RNAs) have only recently been viewed as a target for small-molecules drug discovery. Aminoglycoside compounds are antibiotics which bind the ribosomal A site (16S fragment) and cause misreading of the bacterial genetic code and inhibit translocation. In this work, a complete molecular modeling study is done for 16 newly derived aminoglycoside compounds where diverse nucleoside fragments are linked. Docking calculations are applied to 16S RNA target and a weak linear correlation, between experimental and calculated data, is obtained. However, one particularity of RNA is its high flexibility. To mimic this behavior, all docking calculations are followed by small molecular dynamic simulations. This last computational step improves significantly the correlation with experimental data and allowed us to establish structure–activity relationships. The overall results showed that the consideration of the RNA dynamic behavior is of great interest.

© 2007 Elsevier Masson SAS. All rights reserved.

Keywords: RNA; Aminoglycoside; Antibiotics; Molecular dynamics; Docking

1. Introduction

The potential of RNA as a therapeutic target for small-molecule drug discovery has come to the fore [1–6] with the awareness that RNA molecules can adopt complex three-dimensional structures and then, as like proteins, enable the design of specific ligands. Another reason comes from the biological importance of RNA which is more than a simple copy of genes used temporarily for protein synthesis. Thus, in this biological process, RNA serves as a template (mRNA), ribosome component (rRNA) and an activated intermediate (tRNA). Moreover, RNA also participates in the expression of genes by catalyzing the maturation of mRNAs via

ribosymes. Furthermore, many pathogenic agents, such as retroviruses, encode their genetic information with two identical RNA strands. Considering these essential biological roles, it is surprising to see that RNA has only recently been viewed as a target for structure-based drug design. This is certainly due to the relatively few RNA structural information. However, the number of high-resolution RNA structures has increased significantly during the last decades [7,8] and their advantages over traditional targets have been realized.

The greatest asset of targeting such objects is that RNA usually presents a slower drug resistance development against small molecules. In fact, their functional domains are more highly conserved and pathogens have difficulties to mutate their RNA for developing resilience. Another advantage of targeting this macromolecule comes from its biological role which is diverse and then provides different opportunities and effects. Concerning the cellular translation pathway, RNA is upstream in protein synthesis. Therefore, inhibiting the bacterial RNA ribosome should prevent the formation of thousands of proteins [9].

* Corresponding author. Tel.: +33 1 57 27 68 61; fax: +33 1 57 27 72 63.

** Corresponding author. Tel.: +86 10 82802567; fax: +86 10 82802724.

E-mail addresses: florent.barbault@univ-paris-diderot.fr (F. Barbault), liangren@bjmu.edu.cn (L. Zhang).

✕ Deceased on 22 October 2006.

The large majority of drugs binding to RNA contains positively charged groups. These allow the neutralization of the negatively charged backbone phosphates. Among these cationic compounds we can cite: benzimidazoles [10], cyclophanes [11], diphenyl-furans [12], spermidine–acridine conjugates [13], and the well-known family of aminoglycosides [14–16]. This last family has been known for a long time to be potent antibiotics that bind to specific target sites in the RNA bacterial ribosome [17,18] but also to target group I self-splicing introns [19], the HIV-1 Rev response element RNA [20] and HIV-1 Tar fragment [21], as well as the hammerhead [22] and hepatitis delta virus ribozymes [23].

This work is focused to the antibiotic activity of aminoglycosides. These compounds bind to the 16S ribosomal RNA fragment, which is an essential component of the A site, at an asymmetric internal loop structure [18,24]. This interaction induces codon misreading and inhibits translocation [25,26]. Previous detailed structural studies of the aminoglycosides paromomycin and gentamicin C1A with 16S RNA have provided significant insights of the molecular motifs required to achieve selective RNA recognition [27,28]. The biophysical studies indicate that aminoglycoside-binding to 16S RNA induces a conformational change that stabilizes the 16S rRNA structure [29]. This induced fit effects are slightly different depending on the aminoglycoside ligand.

The use of aminoglycosides as drugs is limited because of their chemical complexity. The design of new, synthetically accessible, analogues is thus necessary. Several compounds formed with a carbohydrate scaffold linked to a nucleoside were designed. The carbohydrates part contains amino groups that are able to interact with the negatively charged phosphate backbone of RNA via electrostatic or hydrogen bonding interactions. The link between the carbohydrate and the nucleoside fragment is an alkyl chain of variable size. The purpose of the nucleoside part is to create an intercalation pattern or form a triple base–pair interaction in the RNA 16S major groove. Table 1 listed the molecular schemes and the binding dissociation constants for RNA 16S [30].¹

Molecular docking is now a widely used technique for the elaboration of new agents and for the elucidation of recognition process [31,32]. However, RNA structures are dynamics and this is fundamental for their functional feature. In the case of RNA 16S, the target plasticity of this macromolecule had been experimentally demonstrated to be essential for the aminoglycoside recognition [29]. Indeed, NMR studies of the free and complexed RNA 16S show that the aminoglycoside induces a local conformational change in the internal loop with the displacement of the two adenine 20 and 21, belonging to the loop, towards the minor groove. Considering this fact, classical docking calculations may have difficulties to provide a correct binding position and energy

since the target is considered rigid throughout the conformational search.

In this paper, we used a combination of molecular docking simulations and small molecular dynamic simulations to mimic the RNA induced fit effect. First, docking studies were done using the 16 compounds listed in Table 1 on the RNA 16S structure. The docking positions' coordinates are then used for small molecular dynamic simulations in implicit water solvent. We showed that the relaxation of the target is an important parameter to take into account in order to achieve a nice correlation between experimental and theoretical binding energies. This final correlation demonstrates the real improvement of this method and allows safer structural interpretations. These analyses are then done for the lead compounds of these new aminoglycoside family and give new insights and information of the recognition process.

2. Materials and methods

2.1. Ligand preparations

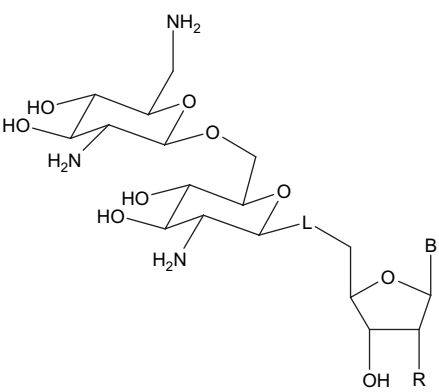


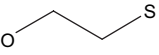
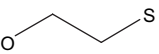
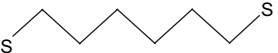
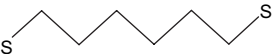
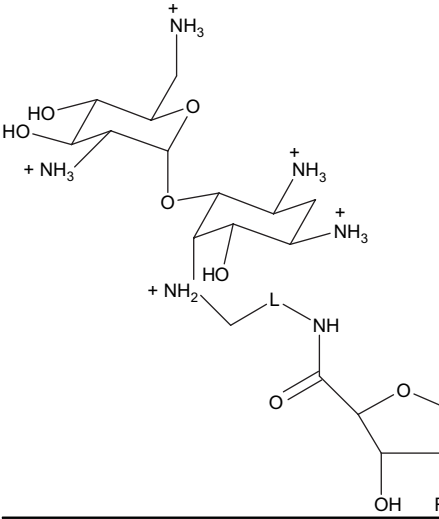
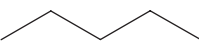
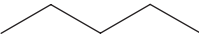
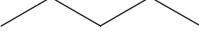
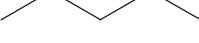
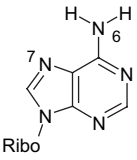
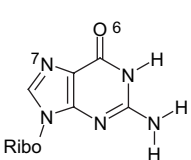
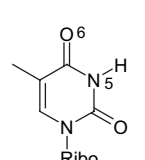
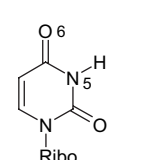
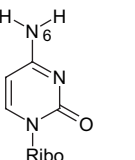
The 16 compounds listed in Table 1 were constructed using the software SYBYL [33] and subjected to 20 simplex iterations followed by 1000 steps of Powell minimization. Since during the molecular docking calculations all rings are rigid a particular attention was made for the cyclohexane rings to reach a correct chair conformation. Moreover, a C3'-endo conformation was applied for the ribose rings of the C, U and A bases whereas a C2'-endo conformation was chosen for the deoxyribose rings of the T bases, according to the RNA and DNA classical sugar puckering conformations [34,35]. For the concerned compounds, the amide conformation was chosen to be *trans* corresponding to the classical observed conformations on small peptides. The *cis* conformations were also tested but never led to lowest energy.

2.2. Molecular docking

The target structure of 16S RNA fragment [28] was extracted from the protein databank (PDB code 1PBR). The Autodock software version 3.0 [36] was used for the molecular docking process. Each dihedral angles were chosen to be flexible in the docking process, even the amide bond in order to mimic the *trans/cis* peptide inversion. Since the scoring function of Autodock has been tested only for protein, a modified set of parameters, suitable for RNA, was used according to a previous work [37]. The grids were constructed around the aminoglycoside experimental ligand positions. The global grids included the residues cytosine 3–10 of one strand and guanine 17–25 of the facing strand (see Fig. 1 for RNA 16S sequence). The Lamarckian Genetic Algorithm method [36] was used for the global optimum binding position search. A number of 200 cycles of calculation (default is 10) was used in order to get a final binding position as accurate as possible. Gasteiger atomic partial charges were used for both RNA and ligands as described in a previous study [37].

¹ The synthesis of the new molecules and experimental data used herein have been published in Dr.'s Ren Bo doctoral thesis (2006, School of Pharmaceutical Sciences, Peking University Health Science Center, University of Peking, P.R.China) and will be further published elsewhere.

Table 1
List of the ligands molecules used in this article

| Scaffold | Name | L | R | B | K _d 16S μM |
|--|--------|---|----|---|-----------------------|
|  | rb0042 |  | OH | U | 1100 |
| | rb0044 |  | H | T | 400 |
| | rb042 | O | OH | U | 2000 |
| | rb044 | O | H | T | 667 |
| | rb092 |  | OH | U | 667 |
| | rb094 |  | H | T | 370 |
| | rb1202 |  | OH | U | 1250 |
| | rb1204 |  | H | T | 117 |
| | rb2402 | C | OH | U | 13 |
| | rb2403 | C | OH | C | 79 |
|  | rb2404 | C | H | T | 9 |
| | rb2405 | C | OH | A | 10 |
| | rb2802 |  | OH | U | 38 |
| | rb2803 |  | OH | C | 104 |
| | rb2804 |  | H | T | 56 |
| | rb2805 |  | OH | A | 17 |
| | | | | | |
| | | | | | |
| | | | | | |
| | | | | | |
| <div>      </div> <div> Adenine (A) Guanine (G) Thymine (T) Uracil (U) Cytosine (C) </div> | | | | | |

The dissociation constants are expressed in μM and have been determined by surface plasmon technique for RNA 16S oligonucleotide.

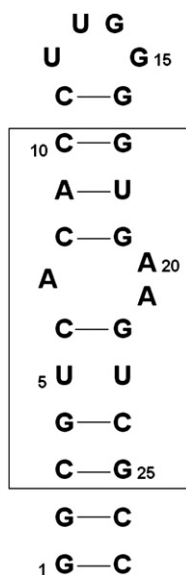


Fig. 1. Secondary structure of the A site RNA 16S used in the molecular modeling study. The residues in the square are those which are taken into account for the molecular docking calculations.

2.3. Dynamics simulations

All molecular dynamics simulations were done with Amber 9.0 package [38]. After the docking process the coordinates of the lowest energy ligand were extracted. Since, the Autodock software works with only polar hydrogens it is necessary to add the missing hydrogens. This is done with the SYBYL software. The antechamber program [39] was used to automatically generate the input file of the ligand coordinates and parameter files. Since electrostatic interactions are essential in RNA molecular recognition, a new set of atomic charges was needed for the molecular dynamics process. Therefore, AM1-BCC (Bond Charge Corrections) charges [40] were computed for each compounds using the Divcon software [41,42]. The final parameters and topology files, used as input for molecular dynamics simulations, were done with the xleap software. The general Amber force field (gaff) [43] was set for the ligand whereas the ff03 [44,45] force field was used for the RNA fragments.

The geometries extracted from the docking calculations were first energy optimized with 500 steps of steepest descent followed by 500 steps of conjugate gradient. A total trajectory of 70 ps at 300 K was made generated by MD simulations: solvent effects were taken into account through general born implicit solvent model [46–49]. The SHAKE algorithm [50] was employed on all covalent bonds containing a hydrogen atom to use a 2 fs time increment. The 1–1 mobile counterions concentration [51] was put to 1 M. The surface area was included in the solvation term and has been computed using the LCPO model [52] (Linear Combinations of Pairwise Overlaps). For all molecular dynamic simulations, the first 20 ps were discarded from the analysis, and so the analyses were done for the last 50 ps mainly with the software ptraj belonging to the Amber package.

2.4. Structural analysis

The structural analysis should not be done on the mean structure, which corresponds to an average of all atomic coordinates. To work with a chemically correct structure it was decided, for all complex, to calculate the RMSD between the trajectory snapshots and the average structure. The considered complex structure is then the conformation which presents the lowest RMSD to the corresponding average structure. We have considered that a hydrogen bond (HB) is present when the donor–acceptor distance is smaller than 3.5 Å and the angle donor–H–acceptor is smaller than 45°. The Visual Molecular Dynamics program [53] was used for the visualisation of trajectories.

3. Results and discussions

3.1. Docking calculation

The docking calculations made in this work are used to generate as correct as possible binding positions of the 16 aminoglycosides ligands onto the RNA 16S target. To do that, the number of docking optimization run cycles is 200 which is high in comparison to HTS (high throughput screening) strategies (from 2 to 10 run cycles) where large database of compounds is docked and then calculation time is a strong limitation. In this work, the molecular dynamic step is largely the more time consuming step, consequently it was chosen to spend more time with docking calculation in order to start MD simulation with the best set of coordinates.

An easy way to evaluate the docking performance is simply to make a correlation between the experimental free energy of binding, extracted from the experimental dissociation constant, and the estimated free energy of binding from the Autodock scoring function. Table 2 summarized these energies and Fig. 2 displays this correlation. The least square correlation is formed and gives a R^2 of 0.702, which is in the best range of those obtained classically [54]. Even if this value is good, several reasons can be drawn in order to improve this result:

- The molecular structures of the 16 compounds are highly flexible, with sometimes 12 torsion angles. This is high for molecular docking where the number of rotatable bonds is a logical limitation for the conformational exploration of the ligand in the active site.
- In molecular docking process with Autodock 3.0 software, there is no evaluation of the internal ligand energy. For this reason the starting ligands' structures should have correct ring conformations since there is no variation of these.
- Finally, it is well known that RNAs are flexible molecules. In the case of 16S RNA target this flexibility has been already demonstrated with the resolution of the apo and complex structure with the aminoglycoside paromomycin [28,29]. The ligand binding induces a local conformational change for the target. Therefore, an induced fit model of interaction should occur for our 16 aminoglycoside compounds and must be taken into account.

Table 2
Experimental and calculated data

| | K_d | ΔG_{exp}^a | Autodock calculations ^b | Average MD interaction energy ^c |
|--------|-------|---------------------------|------------------------------------|--|
| rb0042 | 1100 | −3.94 | −9.0 | −29.4 |
| rb0044 | 400 | −4.52 | −7.3 | −25.9 |
| rb042 | 2000 | −3.59 | −10.4 | −28.8 |
| rb044 | 667 | −4.22 | −12.4 | −26.4 |
| rb092 | 667 | −4.22 | −13.9 | −36.6 |
| rb094 | 370 | −4.56 | −8.1 | −25.8 |
| rb1202 | 1250 | −3.86 | −12.3 | −36.8 |
| rb1204 | 117 | −5.23 | −12.5 | −39.8 |
| rb2402 | 13 | −6.50 | −17.7 | −76.2 |
| rb2403 | 79 | −5.46 | −19.1 | −66.7 |
| rb2404 | 9 | −6.71 | −21.3 | −111.5 |
| rb2405 | 10 | −6.65 | −19.7 | −102.2 |
| rb2802 | 38 | −5.88 | −20.1 | −72.1 |
| rb2803 | 104 | −5.30 | −13.3 | −69.2 |
| rb2804 | 56 | −5.66 | −18.8 | −75.6 |
| rb2805 | 17 | −6.34 | −22.0 | −92.0 |

^a The experimental binding free energy is directly derived from the dissociation constant (see Table 1).

^b Docking free energies are calculated with autodock software and the correlation is plotted in Fig. 2 (left).

^c The average interaction energies are calculated from molecular dynamics simulations and the correlation is plotted in Fig. 2 (right). All units are kcal mol^{−1}.

Considering these points, it seems to be important to add an other simulation step to simulate. Several strategies have been designed to mimic this target flexibility in docking calculations:

- The more simple way is certainly the reduction of the van der Waals force constant. This rough method is easy to implement but it is limited to some sterical adaptations of ligand in the binding pocket [55,56] and may lead to artifacts [56].
- The Slide [57] and FlexE [58] softwares taking into account target flexibility to a certain degree with specific sidechains' relaxations. These informations are obtained from rotamer libraries for the residues' sidechains.

Unfortunately, these programs are only used for protein targets since the conformational information implicates the differentiation between sidechains and backbone atoms, which is impossible for nucleic acids.

- Most efforts for incorporating the target flexibility consist in computational docking with a set of target structures. These can be obtained from several high-resolution structures of the same target bound to different ligands, or in the apo form [59]. Nevertheless, these strategies need the existence of several target structures which represent the different possibilities of binding positions with different ligands and induced fit effects. These experimental data are lacking for this work.

In our case, because the methods listed above are not adequate or need information which are not available, we carried out small molecular dynamic simulations to relax the RNA and ligand and evaluate the induced fit process.

3.2. Molecular dynamics simulations

The major problem to use molecular dynamic as a tool for exploring the recognition process is the huge computational times that these simulations need. For this reason, the trajectory length of all calculation was only 70 ps. This simulation time is not enough for an accurate and reliable molecular movements analysis but enough to observe a system relaxation and structural modifications of the target induced by the ligand. The implicit solvent model was chosen because the computational cost associated with the use of such models in simulations is generally considerably smaller than the cost of representing water explicitly. Indeed, the models describe instantaneous solvent dielectric response which eliminates the need for the lengthy equilibration of water that is typically necessary in explicit water simulations. Due to the absence of viscosity, associated with the explicit water environment, the

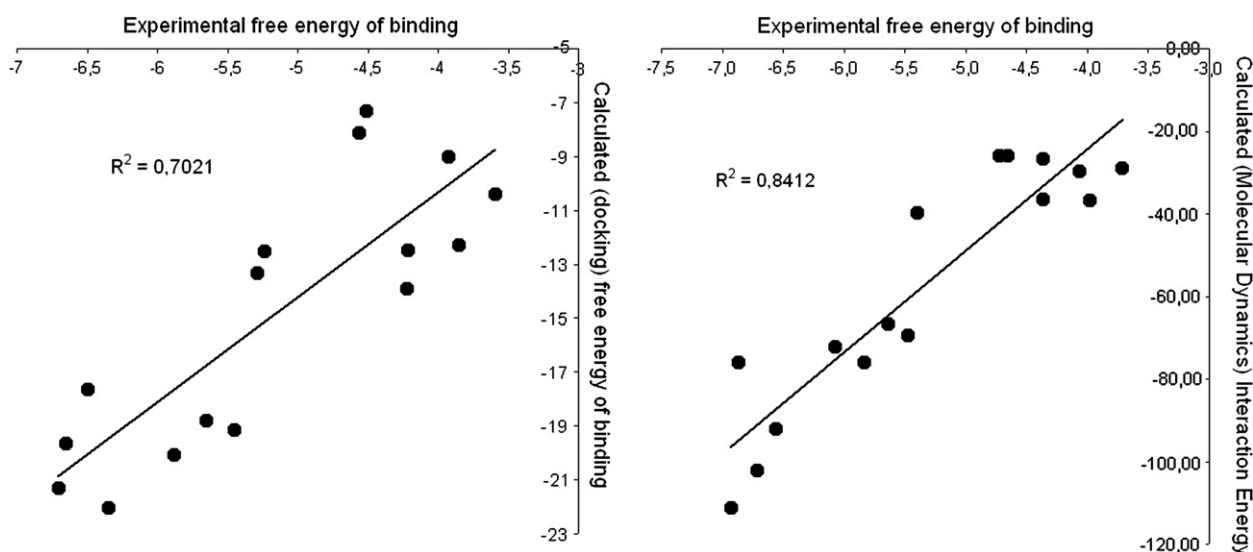
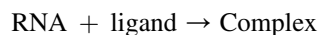


Fig. 2. Linear correlations between experimental free energy and calculated data. (Left) Correlation with the docking binding free energies. (Right) Correlation with the average interaction energies from the molecular dynamics simulations.

molecule may more quickly explore the available conformational space. Moreover, the continuum model corresponds to solvation in an infinite volume of solvent, thereby avoiding possible artefacts of the replica interactions that occur in the periodic systems typically used for explicit water calculations. However, with this method it is impossible to see direct interaction of water molecules like hydrogen bonds.

To calculate the interaction energy for each ligand, three molecular dynamics calculations were launched for each compound, one for the complex structure extracted from the previous docking calculation, one for the ligand alone and the last one for the target alone. The interaction energy (E_{int}) is obtained from the total energy of all species according to the following equations:



$$E_{\text{int}} = E_{\text{complex}} - E_{\text{RNA}} - E_{\text{ligand}}$$

These energies data are shown in Table 2. A correlation graph with the experimental free energy and calculated interaction energy is done and the linear regression can be directly compared to that obtained from the docking calculation. The final R^2 coefficient is 0.84, which is indubitably better than simply with the docking calculations and largely better than the correlations found in the literature [54]. Therefore, the use of target flexibility gives a real improvement in the exploration of the recognition process. The interpretation of the complex structures and the elaboration of structure–activity relationships are consequently more safe and accurate.

3.3. Structural activity relationships analysis

Molecular dynamics offers more than a single structure but takes into account the molecular movements. Although the equilibration and production times are too weak in comparison to the complexity of such 16S RNA systems, the purpose of these molecular dynamics was not to elucidate molecular movements but to give the necessary flexibility in the systems to reach a correct interaction structure. For this reason, the hydrogen bonding network discussed below is observed all along the 50 ps trajectory.

All ligand molecular affinities are compiled in Table 1. The R^2 coefficient indicates that our model is reliable. However, among all molecules, some are not of biological interest to evaluate. So, this analysis is only focused on molecules which present a dissociation constant below 400 μM . Moreover, to do a coherent structural analysis, it is essential to make comparisons with molecules displaying discrepancies of more than 1 kcal mol^{-1} differences in experimental free energy of bindings. This value is directly imposed by the force field accuracy. Consequently to all the above conditions, the following structural analysis is only focused on molecules rb2404 or rb2405 vs rb2403 and rb2803 vs rb2805.

3.4. rb2404 and rb2405 compared to rb2403

rb2404 and rb2405 are potentially the more active molecules with dissociation constant of 9 and 10 μM , respectively.

Despite these identical affinities, the structures of these compounds are different for the nucleoside part with an adenine purine base for rb2405 and a pyrimidine thymidine base for rb2404. rb2403 compound presents an interesting features with a cytosine base for the nucleoside part but a lowest affinity to RNA 16S (79 μM). These two compounds, and rb2403, display positives charges on all amino groups which lead to a global net charge of +5.

Fig. 3 shows the interaction patterns for these three compounds. The common aminoglycoside part is placed identically in all structures. As expected, some ammonium groups strongly interact with the RNA phosphate negative charges leading to strong electrostatic interaction and an identical placement of this scaffold for these three compounds. More precisely, the aminoglycoside part is placed on the major groove of the RNA 16S structure where the two ammonium functions of the glucose part are interacting with phosphate groups of residues A7 and U18 of the two facing strands. The cyclohexane ring is carrying three ammonium groups, the equatorial ones are near the residues G4 and U5. The ammonium in axial conformation of this cyclohexane fragment is strong hydrogen bonded with the N7 atom of G19 on the major groove. This electrostatic effect induces a narrowing of the major groove with the two facing strands. These last structural implications were not obtained from the docking calculations and most probably result from the target flexibility. Thus, the nucleoside part is oriented towards this groove and allows the creation of base–base or base–backbone interactions. Therefore, the three molecules' interaction energy variations depend only on the interaction types of these nucleoside fragments.

For rb2404 compound, the imino group of thymine base is making a hydrogen bond with the O2 atom of the residue cytosine 3 phosphate group, whereas the hydroxyl group on the deoxyribose unit is making a hydrogen bond with the O2 atom of the residue adenine 20 phosphate group. These two supplementary hydrogen bonds induced the orientation and limit the molecular movement of the nucleoside part.

rb2405 presents an adenine on the nucleoside part which is a bulkier group in comparison to the thymine for rb2404. Like for rb2404, two hydrogen bonds are observed for this nucleoside part: the amino group of adenine (N7) is making a hydrogen bond with the O2 atom of the residue guanine 22 and an other hydrogen bond with the base N7 atom of the same residue. The same number of hydrogen bonds explains the identical affinity with RNA 16S for these two molecules and are represented with a neighboring MD average interaction energy of $-111.5 \text{ kcal mol}^{-1}$ for rb2405 and $-102.2 \text{ kcal mol}^{-1}$ for rb2404.

The rb2403 case is interesting since the chemical structure is similar to rb2404 with a pyrimidine type nucleoside. Indeed, rb2403 displays a cytosine base on the nucleoside fragment whereas it is a thymidine for rb2404. The amino group of cytosine is making a hydrogen bond with the O2 atom of the residue cytosine 3 phosphate group. This hydrogen bond is then identical for rb2403 and rb2404 but there is no observation, along the trajectory, of a hydrogen bond on the other strand like there is with the hydroxyl group of the deoxyribose

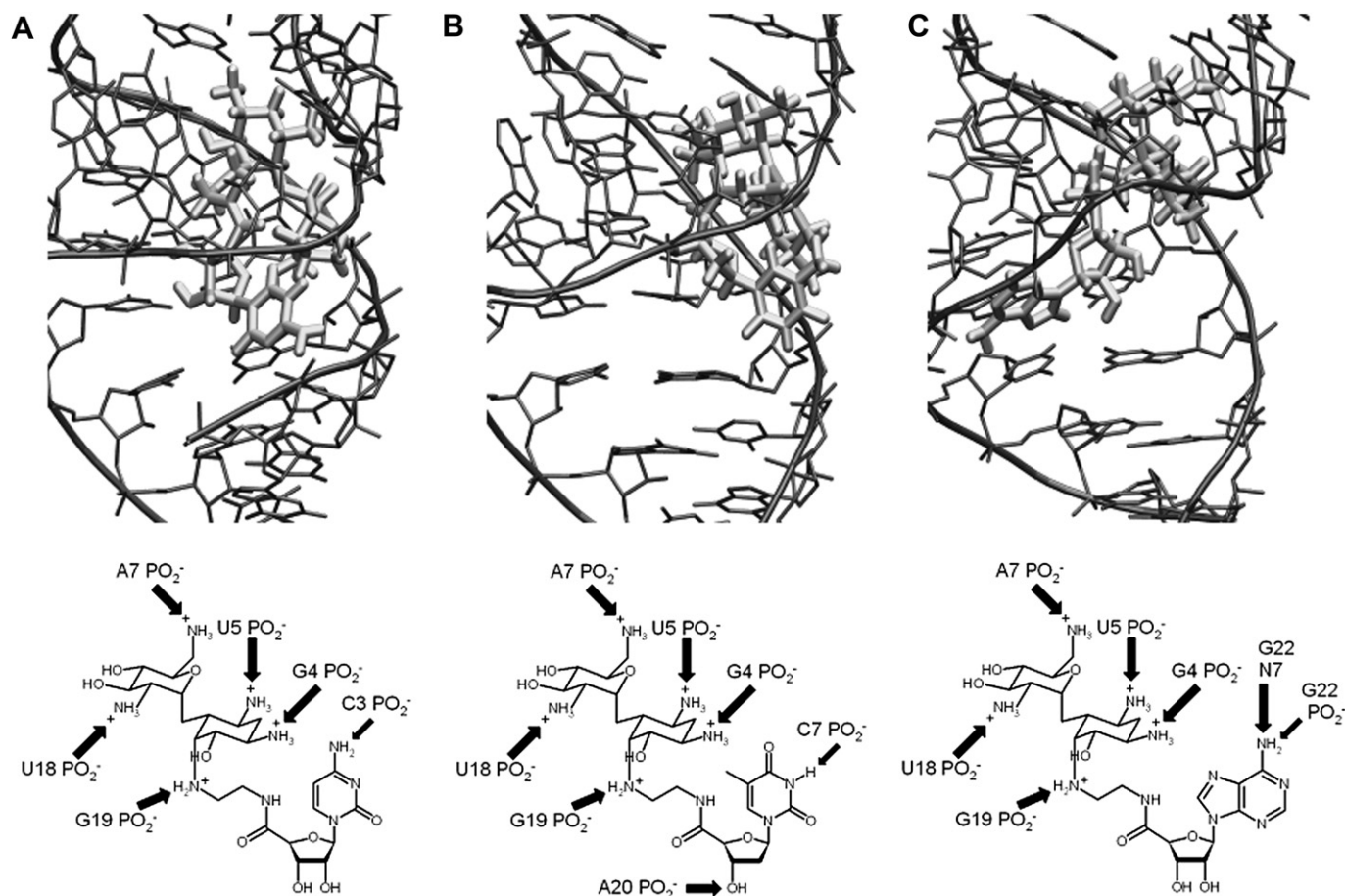


Fig. 3. Molecular dynamics structural information for ligands rb2403 (A), rb2404 (B) and rb2405 (C). On the top, zoom of the interactions on RNA 16S active site. On the bottom, schemes of the interactions.

fragment of rb2404. This hydrogen bond leaking is confirmed by the observation of the MD average interaction energies: rb2403 displays $-66.7 \text{ kcal mol}^{-1}$ whereas rb2404 and rb2405 present, respectively, -102.2 and $-111.5 \text{ kcal mol}^{-1}$.

The explanation which can be drawn is that the position of the base hydrogen bond with the phosphate group of cytosine 3 is essential for a correct orientation of a hydroxyl group to make the second hydrogen bond with the O2 atom of phosphate A22. The amino and imino functions in base cytosine and thymidine are placed on different positions on the pyrimidine ring and induced this globally different position for the nucleoside fragment onto RNA 16S. The bottom part of Fig. 3 summarizes the interaction patterns with a specific scheme for all the three structures. These slight structural differences among rb2403, rb2404 and rb2405 are not accessible only with the docking calculations where the structural positions of these compounds are similar. The molecular dynamics gave enough flexibility to the systems to observe these different interaction behaviors.

3.5. rb2803 compared to rb2805

Like for the rb24 set, rb2803 and rb2805 compounds present five positives charges and are involved in electrostatic

interactions with the RNA backbone negatives charges. Rb2803 and rb2805 are composed of a common aminoglycoside fragment, identical to rb24 series discussed above. A major difference is seen for the aliphatic linking part of rb28 type compounds with six supplementary carbons for these molecules. rb2803 and rb2805 differ only on the nucleoside part with an adenine and a cytosine base, respectively. Despite these chemical similarities, rb2803 and rb2805 present a significant affinity variation with a dissociation constant value of $17 \text{ }\mu\text{M}$ for rb2805 and $104 \text{ }\mu\text{M}$ for rb2803. The average interaction energies of rb2805 and rb2803 are, respectively, -92.0 and $-69.2 \text{ kcal mol}^{-1}$ which represent the selectivity variation of these two ligands.

Like observed previously for the rb24 ligands, the rb2803 and rb2805 overall position on the RNA 16S major groove is identical. Fig. 4 summarizes all the interactions discussed here. The glucose fragment ammonium groups are facing the cytosine 6 residue phosphate group and provide a hydrogen bond with the O6 atom of the guanine 19 base. Concerning the cyclohexane ring, their ammonium charges are eclipsing the phosphate negative charges of guanine 17, uracil 5 and 18 residues. All these strong electrostatic interactions are responsible for the stable position onto the RNA 16S fragment of rb2803 and rb2805. It can be noticed that the global position

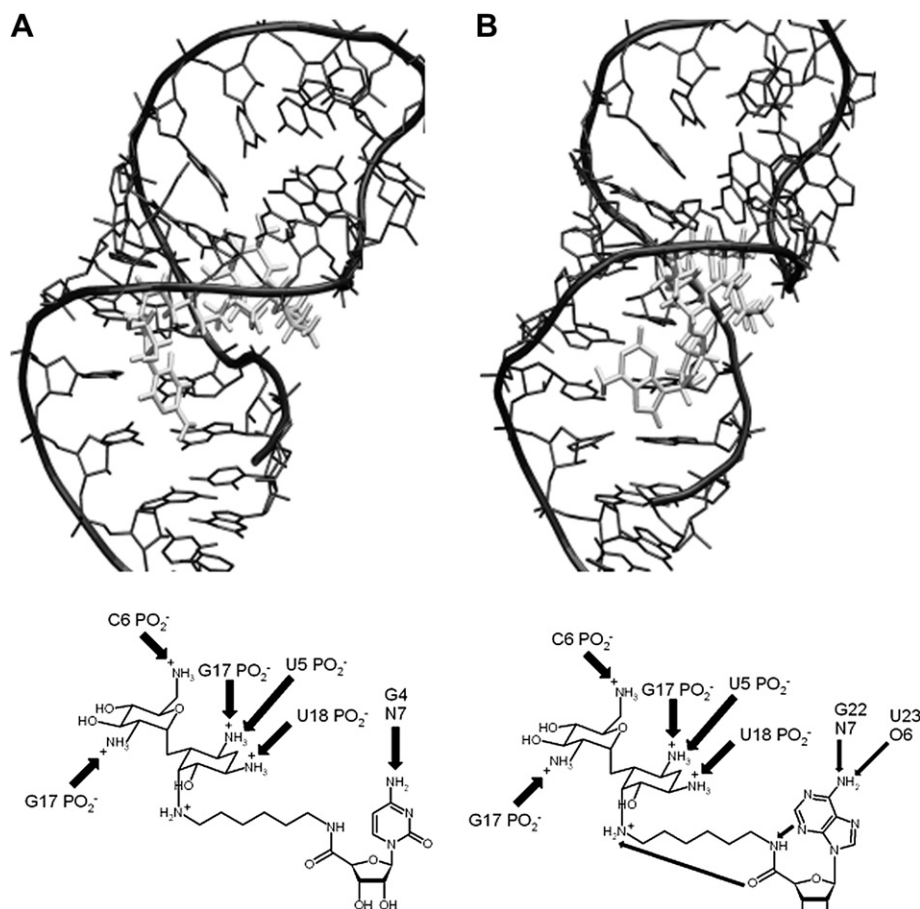


Fig. 4. Molecular dynamics structural information for ligands rb2803 (A) and rb2805 (B). On the top, zoom of the interactions on RNA 16S active site. On the bottom, schemes of these interactions.

of this aminoglycoside part is similar to the one observed with the rb24 compounds, there is only a slight translation towards the major groove, but the overall orientation is identical. Indeed, the location of this fragment on the RNA 16S major groove permits a similar overall orientation of the nucleoside and the aliphatic link parts.

Again, the only difference between rb2803 and rb2805 is the nucleoside part. For rb2805 an adenine is present and this amino group (N6) provides two hydrogen bonds with the N7 atom of guanine 22 and the O6 atom of the uracil bases. Because of these two hydrogen bonds on sequential residues (22 and 23) the position of the adenine is perpendicular to the RNA stem base pairs. Moreover, this nucleoside location stabilizes the adenine nucleoside position and then limits the aliphatic link movements. Two internal hydrogen bonds are then observed, the first one concerned the cyclohexane equatorial ammonium group which makes a strong hydrogen bond with the oxygen of the amide group. This hydrogen bond limits drastically the flexibility of this aliphatic link. The second internal hydrogen bond involves the NH amide atom with the N3 atom of the adenine base. This last interaction is possible only because the adenine is placed perpendicular to the stem and then induced a displacement of the chi dihedral angle (chi torsion angle is defined between the base and the ribose fragment) from the classical *anti* to *syn* position.

For rb2803, only one hydrogen bond is observed. This one is placed between the amino group of cytosine and the N7 atom of guanine 4. Therefore, the nucleoside fragment position is not identical to rb2805 one (Fig. 4) and the aliphatic chain is elongated on the RNA groove making hydrophobic interactions. However, these last interactions provide less binding energy and explain the dissociation constants' variations. Fig. 4 summarized the interaction patterns for rb2803 and rb2805. Like for rb2403, rb2404 and rb2405, the slight differences of nucleosides placement in the RNA 16S major groove are accessible only after the molecular dynamics simulations. This molecular modeling step is therefore necessary to observe the mutual movements of the nucleoside fragment and the RNA 16S target to establish the hydrogen bonding network.

Among all these structural implications it is important to point out the fact that rb2403, rb2404 and rb2803, rb2805 aminoglycoside parts are always placed in the same way onto the RNA 16S fragment. Some years ago, this specific placement has been defined to be at the origin of the antibiotic action of gentamicin [22] and extended to the overall role of aminoglycoside compounds. Similar conclusions can be drawn here, with a position of the aminoglycoside part essential for RNA 16S inhibition. The nucleoside fragment is then used for modulating the affinity of these anti-microbial compounds.

4. Conclusions

This work was focused on the theoretical interaction studies of 16 new aminoglycoside compounds to the RNA 16S ribosomal bacterial structure. We have shown, by using a combination of molecular docking calculations followed by small molecular dynamics simulations, that the relaxation of the RNA target is an important parameter to take into account. This method gave us a nice correlation between calculated average interaction energies and experimental gibbs energies. This good result allowed safer structural analysis of several typical aminoglycoside compounds among the 16. The overall structural analysis concluded that the ligands positive global charge is one of the major parameter to control. The nucleoside fragment, belonging to this aminoglycoside family, induces the affinities variations against RNA 16S by various hydrogen bonding networks.

The design of new aminoglycoside antibiotics with highest affinity is of great interest in modern medicinal chemistry. It is hope that the present work will help to accomplish this objective.

Acknowledgements

The works of the Ph.D. students are supported by various fellowships: Joseph Rebehmed from the French Ministry of Research and Technology, Catia Teixeira from the “Fundação para a Ciência e a Tecnologia” of Portugal and Yun Luo from the French Embassy. This work is also supported by The Ministry of Science and Technology of China (Grant No. 2004CB518904 to Lihe Zhang) and National Natural Science Foundation of China (Grant No. 90713005 to Liangren Zhang). This work is dedicated to the memory of Professor BoTao Fan, died on 22 October 2006, who initiated this project.

References

- [1] C. Chow, F. Bogdan, *Chem. Rev.* 97 (1997) 1489–1513.
- [2] N. Pearson, C. Prescott, *Chem. Biol.* 4 (1997) 409–414.
- [3] T. Hermann, E. Westhof, *Curr. Opin. Biotechnol.* 19 (1998) 66–73.
- [4] D. Ecker, R. Griffey, *Drug Discov. Today* 4 (1999) 420–429.
- [5] Y. Tor, *Angew. Chem., Int. Ed.* 38 (1999) 1579–1582.
- [6] S. Sucheck, C.-H. Wong, *Curr. Opin. Chem. Biol.* 4 (2000) 678–686.
- [7] R. Batey, R. Rambo, J. Doudna, *Angew. Chem., Int. Ed.* 38 (1999) 2326–2343.
- [8] A. Ramos, C. Gubser, G. Varani, *Curr. Opin. Struct. Biol.* 7 (1997) 317–323.
- [9] T.K. Ritter, C.H. Wong, *Angew. Chem., Int. Ed. Engl.* 40 (2001) 3508–3533.
- [10] W. Wilson, L. Ratmeyer, M. Zhao, L. Strekowski, D. Boykin, *Biochemistry* 32 (1993) 4098–4104.
- [11] M. Fernandez-Saiz, H. Schneider, J. Sartorius, W. Wilson, *J. Am. Chem. Soc.* 118 (1996) 4739–4745.
- [12] W. Wilson, L. Ratmeyer, M. Zhao, D. Ding, A. Mc Connaughie, A. Kumar, D. Boykin, *J. Mol. Recogn.* 9 (1996) 187–196.
- [13] F. Hamy, V. Brondani, A. Flörsheimer, W. Stark, M. Blommers, T. Klimkait, *Biochemistry* 37 (1998) 5086–5095.
- [14] Y. Wang, R. Rando, *Chem. Biol.* 2 (1995) 281–290.
- [15] T. Hermann, E. Westhof, *J. Med. Chem.* 42 (1999) 1250–1261.
- [16] R. Schroeder, U. von Ahsen, *Nucleic Acids Mol. Biol.* 10 (1996) 53–74.
- [17] H. Noller, *Annu. Rev. Biochem.* 60 (1991) 191–227.
- [18] S. Moazed, H. Noller, *Nature* 327 (1987) 389–394.
- [19] H. Wank, J. Rogers, J. Davies, R. Schroeder, *J. Mol. Biol.* 236 (1994) 1001–1010.
- [20] M.L. Zapp, S. Stern, M.R. Green, *Cell* 74 (1993) 969–978.
- [21] C. Faber, H. Stricht, K. Schweimer, P. Rösch, *J. Biol. Chem.* 275 (2000) 20660–20666.
- [22] T. Hermann, E. Westhof, *J. Mol. Biol.* 276 (1998) 903–912.
- [23] J. Rogers, A.H. Chang, U. von Ahsen, R. Schroeder, J. Davies, *J. Mol. Biol.* 259 (1996) 916–925.
- [24] J. Woodcock, S. Moazed, M. Cannon, J. Davies, H. Noller, *EMBO J.* 10 (1991) 3099–3103.
- [25] J. Davies, L. Goroni, B. Davis, *Mol. Pharmacol.* 1 (1965) 93–106.
- [26] J. Davies, B. Davis, *J. Biol. Chem.* 243 (1968) 3312–3316.
- [27] S. Yoshizawa, D. Fourmy, J. Puglisi, *EMBO J.* 17 (1998) 6437–6448.
- [28] D. Fourmy, M. Recht, S. Blanchard, J. Puglisi, *Science* 274 (1996) 1367–1371.
- [29] D. Fourmy, S. Yoshizawa, J. Puglisi, *J. Mol. Biol.* 277 (1998) 333–345.
- [30] L. Cai, Q. Li, B. Ren, Z.-J. Yang, L. Zhang, L. Zhang, *Tetrahedron* 63 (2007) 8315–8144.
- [31] P. Lyne, *Drug Discov. Today* 7 (2002) 1047–1055.
- [32] P. Gane, P. Dean, *Curr. Opin. Struct. Biol.* 10 (2000) 401–404.
- [33] SYBYL. 7.0, Tripos Inc., 1699 South Hanley Rd., St Louis, Missouri 63144, USA.
- [34] S. Neidle (Ed.), *Oxford Handbook of Nucleic Acid Structure*, Oxford Science Publications, Oxford, 1999.
- [35] W. Saenger (Ed.), *Principles of Nucleic Acid Structure*, Springer, New York, 1984.
- [36] G.M. Morris, D.S. Goodsell, R. Huey, A.J. Olson, *J. Comput. Chem.* 19 (1998) 1639–1662.
- [37] F. Barbault, L. Zhang, L. Zhang, B. Fan, *Chemom. Intell. Lab. Syst.* 82 (2006) 269–275.
- [38] D. Case, T. Darden, T. Cheatham, C. Simmerling, J. Wang, R. Duke, R. Luo, K. Merz, D. Pearlman, M. Crowley, R. Walker, W. Zhang, B. Wang, S. Hayik, A. Roitberg, G. Seabra, K. Wong, F. Paesani, X. Wu, S. Brozell, V. Tsui, H. Gohlke, L. Yang, C. Tan, J. Mongan, V. Hornak, G. Cui, P. Beroza, D. Mathews, C. Schafmeister, W. Ross, P. Kollman, *AMBER, 9.0*, University of California, San Francisco, 2006.
- [39] J. Wang, W. Wang, P. Kollman, D. Case, *J. Mol. Graph. Model.* 25 (2006) 247–260.
- [40] M. Dewar, E. Zebisch, E. Healy, J. Stewart, *J. Am. Chem. Soc.* 107 (1985) 3902–3909.
- [41] A. Jakalian, D. Jack, C. Bayly, *J. Comput. Chem.* 23 (2002) 1623–1641.
- [42] A. Jakalian, B. Bush, D. Jack, C. Bayly, *J. Comput. Chem.* 21 (2000) 132–146.
- [43] J. Wang, R. Wolf, J. Caldwell, P. Kollman, D. Case, *J. Comput. Chem.* 25 (2004) 1157–1174.
- [44] M. Lee, Y. Duan, *Proteins* 55 (2004) 620–634.
- [45] Y. Duan, C. Wu, S. Chowdhury, M. Lee, G. Xiong, W. Zhang, R. Yang, P. Cieplak, R. Luo, T. Lee, *J. Comput. Chem.* 24 (2003) 1999–2012.
- [46] C. Cramer, D. Truhlar, *Chem. Rev.* 99 (1999) 2161–2200.
- [47] P. Beroza, D. Case, *Meth. Enzymol.* 295 (1998) 170–189.
- [48] J. Madura, M. Davis, M. Gilson, R. Wade, B. Luty, J. Mc Cammon, *Rev. Comput. Chem.* 5 (1994) 229–267.
- [49] M. Gilson, *Curr. Opin. Struct. Biol.* 5 (1995) 216–223.
- [50] J.P. Ryckaert, G. Ciccotti, H.J.C. Berendsen, *J. Comput. Phys.* 23 (1977) 327–341.
- [51] J. Srinivasan, M. Trevathan, P. Beroza, D. Case, *Theor. Chem. Acc.* 101 (1999) 426–434.
- [52] J. Weiser, P. Shenkin, W. Still, *J. Comput. Chem.* 20 (1999) 217–230.
- [53] W. Humphrey, A. Dalke, K. Schulten, *J. Mol. Graph.* 14 (1996) 33–38.
- [54] R. Wang, Y. Lu, S. Wang, *J. Med. Chem.* 46 (2003) 2287–2303.
- [55] V. Schnecke, C.A. Swanson, E.D. Getzoff, J.A. Tainer, L.A. Kuhn, *Proteins* 33 (1998) 74–87.
- [56] D.A. Gschwend, A.C. Good, I.D. Kuntz, *J. Mol. Recognit.* 9 (1996) 175–186.
- [57] V. Schnecke, L. Kuhn, *Perspect. Drug Discov. Des.* 20 (2000) 171–190.
- [58] H. Claussen, C. Buning, M. Rarey, T. Lengauer, *J. Mol. Biol.* 308 (2001) 377–395.
- [59] R.M. Knegtel, I.D. Kuntz, C.M. Oshiro, *J. Mol. Biol.* 266 (1997) 424–440.